Journal of Electrochemical Science and Technology
Vol. 4, No. 3, 2013, 113-118
http://dx.doi.org/10.5229/JECST.2013.4.3.113

Journal of Electrochemical Science and Technology

Electrochemical Characteristics of Nano-sized A_2MnPO_4F (A = Li, Na) as Cathode Materials for Lithium ion Batteries

Woosuk Cho, Jun Ho Song, Sang-Min Kim, Dong-Jin Kim, Min-Gu Kang,
Jeom-Soo Kim*, and Young-Jun Kim

Advanced Batteries Research Center, Korea Electronics Technology Institute, #68 Yatap-dong, Bundang-gu, Seongnam-si, Gyeonggi-do 463-816, Korea

ABSTRACT

Fluorophosphate, Na_2MnPO_4F as new cathode material was synthesized by carbothermal treatment method. Prepared Na_2MnPO_4F has particle size under 100 nm and residual carbon exists in surface of Na_2MnPO_4F. Additional carbon coating was performed in order to increase the electrochemical properties. Even capacity and overpotential were improved by carbon coating using mechanical ball milling, the reduced crystallinity limited the drastic improvement of the electrochemical properties. To solve this problem, re-heat treatment was involved to recover crystallinity and then notable improvement of electrochemical properties was obtained. Specific amount of Li^+ that participates in electrochemical Li^+ insertion / extraction reaction, was x = 1 in $Li_xNa_{2-x}MnPO_4F$ within the voltage range of 2.0 to 4.8 V. The doubled capacity by 2 electron reaction can be obtained when NMPF is charged to higher voltage over 4.8 V.

Keywords: Na_2MnPO_4F, Fluorophosphate, Cathode, Li ion batteries

Received September 7, 2013 : Accepted October 17, 2013

1. Introduction

Lithium ion battery (LIB) has been successfully used for power sources of mobile information technology (IT) devices. The application field of LIB has been extended to automobile field such as electric vehicles (EVs) and hybrid electric vehicles (HEVs) in recent year. Higher energy and power density will be required for successful launch of LIB in this field.[1,2] To overcome this issue, new cathode materials with high energy density are widely researched.

Fluorophosphates, A_2MPO_4F (A = Li, Na, M = Fe, Co, Ni, Mn) contains 2 lithium or sodium ions in the tunnel sites. Comparing to olivine $LiMPO_4$ (M = Fe, Mn) materials, theoretical capacity of A_2MPO_4F is double due to 2 electron reaction per unit formula, if all alkali metal ions are inserted / extracted in host structure.[3-10] For Mn based fluorophosphates, A_2MnPO_4F (A = Li and/or Na), direct synthesis of Li based Li_2MnPO_4F has not been reported in the best of our knowledge. Na based Na_2MnPO_4F is only directly prepared for Mn based fluorophosphate.[4,5] Therefore, Li contained $Li_xNa_{2-x}MnPO_4F$ ($0 \le x \le 2$) can be prepared by electrochemical or chemical Li^+ insertion into Na_2MnPO_4F.[10] Na_2MnPO_4F can also be considered as a cathode material for Na ion battery (NIB). However, the possibility of using it for LIB has been investigated in this study because the energy of cell applied Na_2MnPO_4F is higher in case of LIB resulted from the higher reaction voltage of Li^+.

Na_2MPO_4F belongs to the space group of $P2_1/n$, which is constructed of a framework and 3-dimentional tunnel parts. The framework consists of MnO_4F_2 octahedrons and PO_4 tetrahedrons linkage as shown in Fig. 1. However, such a point shared linkage

*Corresponding author. Tel.: +82-31-789-7491
E-mail address: js_energy@keti.re.kr

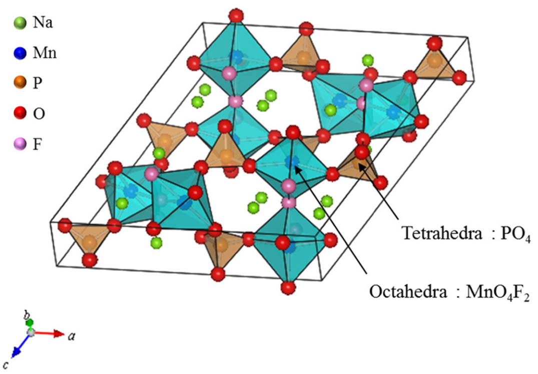

Fig. 1. Crystal structure of the fluorophosphates A_2MPO_4F (A = Li, Na).

of polyhedron induces the low electric conductivity.[11] Poor electrochemical activity due to low electric conductivity limits this material to be used as a cathode material for Li-ion battery.[4,5] It is expected that nano-sized particle provides a short diffusion pathway and large surface area. Especially, the effective carbon coating is possible due to large surface area.[12-14] Therefore, improvement of electric activity will be achieved by nano-sized materials.

In this study, nano-sized Na_2MnPO_4F was synthesized by carbothermal treatment method and additional carbon coating was performed to improve the electrochemical activity of Na_2MnPO_4F. The structure, morphology, and electrochemical properties of the NMPF prepared by carbothermal treatment method were investigated.

2. Experimental

NMPFs were synthesized by using carbothermal treatment (CT) method and conventional solid state reaction in order to obtain different particle size. For CT method, NaF, Na_2CO_3, MnC_2O_4-$2H_2O$, and $(NH_4)_2HPO_4$ were used as starting materials, and citric acid was used as the carbon source. The starting materials are mixed by planetary ball milling at 400 rpm for 6h then heated at 300°C for 2h under air atmosphere to remove CO_2, H_2O, and NH_3. After this step, the obtained precursor and 20 wt.% of citric acid were mixed with hexane solvent then ball milling was performed at 400 rpm for 24h. Finally the mixed material was annealed at 500°C for 6h under Ar atmosphere. For solid state reaction, same starting materials as CT method were used. The starting materials are mixed by planetary ball milling at 400 rpm for 6h then heated at 300°C for 2h under air atmosphere. The obtained powder was grounded then reheated at 650°C for 6h under Ar atmosphere.

Structural information was obtained by X-ray diffraction (XRD) measurement using Empyrean diffractometer (PANalytical) equipped with monochromated Cu Kα radiation (λ = 1.54056 Å). Lattice parameter was calculated by Rietveld refinement. The powder morphology and particle size were characterized by field-emission scanning electron microscopy (FESEM, JEOL JSM-7000F). The amount of residual carbon of NMPF prepared by CR method was measured by CHNSO elemental analysis (ECS 4010, Costech INC.).

The electrodes were prepared by coating slurries containing active material powders (80 wt.%), carbon black (Super P, 10 wt.%), and polyvinylidene fluoride (PVDF, 10 wt.%) dissolved in n-methyl-2-pyrrolidone (NMP). After coating, the electrodes were pressed and dried for 12 h at 120°C. Coin-type cells (CR 2032) were assembled in a dry room with the dew point controlled to less than –45°C. The cells consisted of the NMPF working electrode, a Li metal foil counter electrode, a porous polyethylene membrane separator, and 1 M $LiPF_6$ dissolved in ethylene carbonate (EC) and dimethyl carbonate (DMC) (1:2 in volume ratio) as the electrolyte (Panax Etec). The electrochemical properties were performed galvanostatically at a constant current C/20 in the voltage range of 2.0~4.8 V using a TOSCAT-3100U cycler (Toyo system Co.).

3. Results and Discussion

Powder XRD patterns of NMPF prepared by CT method (hereafter, call as CT NMPF) are show in Fig. 2, together with a simulated XRD pattern using structural data reported by Olga et al. (ref. in inorganic crystal structure database, ICSD #59301).[15,16] Both patterns are good accordance with a single phase of orthorhombic $P2_1/n$ structure without any impurity phase. The lattice parameters are obtained by Rietveld refinement using RIETAN-FP software.[17] The refined lattice parameters are shown in Table 1 and values are consistent with those of reported NMPF structure.[15] Single phase of NMPF is synthesized well by CT method using citric acid as carbon source within detection limit of XRD.

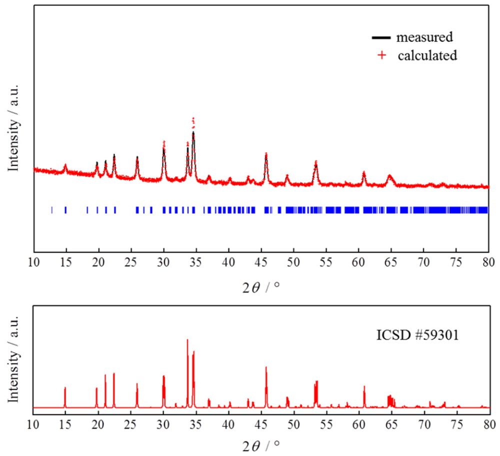

Fig. 2. X-ray diffraction pattern of NMPF with refined pattern.

Table 1. Refined lattice parameters of Na_2MnPO_4F (CT NMPF)

	a (Å)	*b* (Å)	*c* (Å)	*β* (°)
Lattice parameter	13.693	5.317	13.760	120.058

The colors of NMPF powders prepared by CT method (CT NMPF) and solid state reaction (SS NMPF) indicate white and black, respectively, which indicate the residual carbon exists in CT NMPF particles. Therefore, the CT NMPF prepared by CT method exists as NMPF/C composite. The CHNO elemental analysis was performed to determine the amount of carbon and quantitative amount of carbon is 3 wt.% in CT NMPF. In the XRD pattern, no visible reflection of carbon is observed, which indicates that carbon in CT NMPF exists as an amorphous phase. These residual carbons are expected to be uniformly distributed over the NMPF particles, which may enhance the electron moving pass.

FESEM images of the CT NMPF and SS NMPF are shown in Fig. 3. In contrast to the primary particle size with 2 μm for SS NMPF, the primary particle size of CT NMPF is less 100 nm. Although the secondary particle morphology consists of aggregates of primary particles, the primary particles show almost same size and morphology. In general, CT method provides relatively low synthesis temperature by annealing with carbon source in an inert atmosphere, which suppresses the particle growth.[14,18,19] On the basis of the above results, nano-sized NMPF was prepared successfully by the CT method.

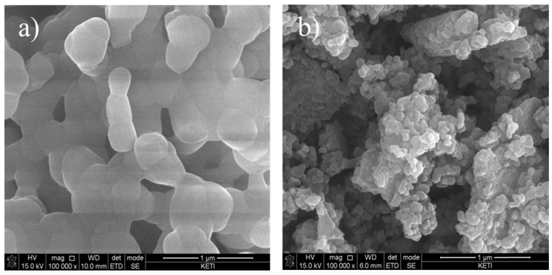

Fig. 3. FESEM images of NMPF prepared by a) solid state reaction, and b) CT method.

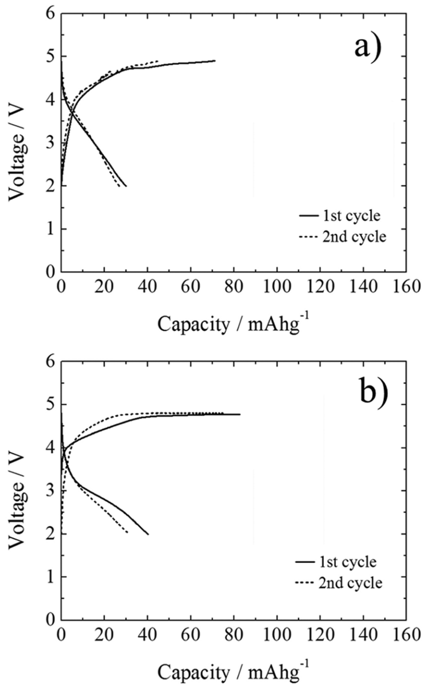

Fig. 4. Charge-discharge profiles for a) SS-NMPF, and b) CT-NMPF.

NMPF electrodes were used to perform the electrochemical Li^+ insertion/extraction reaction. Na ions are electrochemical extracted from NMPF at first charging step, and then Li ions are inserted into Na site (x in $Li_xNa_{2-x}MnPO_4F$) from following discharging process.

To investigate the size effect of NMPF for electrochemical properties, NMPF electrodes were prepared by using nano-sized CT NMPF and micro-sized SS NMPF powders. Galvanostatic charge-discharge cycling was performed in voltage range of 2.0 V to 4.8 V with C-rate of C/20. Charge-discharge profiles during 2 cycles are shown in Fig. 4.

In case of SS NMPF, discharge capacity is 30 $mAhg^{-1}$ and no obvious voltage plateau is observed. For CT NMPF, discharge capacity is 40 $mAhg^{-1}$ and voltage profile is slightly improved to compare SS-NMPF. It can be assumed that nano-sized particle provides the short pathway of Li^+ diffusion and large surface area, which serves high reactivity of Li^+ insertion. Even, the enhanced electrochemical activity is expected for CT NMPF, the cell performance is still not enough to use CT NMPF as cathode. On the basis of above results, NMPF has the electric conductivity as low as insulator, and it is confirmed that improvement of electrochemical properties of NMPF is limited only through the reducing particle size. Therefore, additional carbon coating such for olivine type $LiFePO_4$ will be required in order to improve electrochemical activity of NMPF.[12,13)]

25 wt.% of Super-P was added to CT NMPF then mixture were ball-milled for 6h (hereafter, called CT-A NMPF). The galvanostatic charge-discharge profile of CT-A NMPF is shown in Fig. 5. After carbon coating, discharge capacity is dramatically increased to 68 $mAhg^{-1}$ and overpotential during discharge is also improved. It is expected that nano-sized particles provide the large surface area that induce the effective area of carbon coating.[13)] Furthermore, the increase of electric conductivity is expected by the creating of electric network between Super-P and residual carbon on surface and/or grain boundary of NMPF.

Even electrochemical properties of CT-A NMPF is improved by effective carbon coating, the average working voltage and capacity are not reached to the expected value of 4.0 V and 302 $mAhg^{-1}$(for two Li^+ intercalation; two electron reaction), respectively.

Additional carbon coating requires the mechanical ball milling process. The decrease of crystallinity will be expected through the ball milling process, which can disturb to reveal the original performance of material. In order to confirm the crystallinity of CT-A NMPF, XRD measurement was performed and XRD patterns are shown in Fig. 6. As we respect, XRD pattern of CT-A NMPF presents the reduced intensity and larger peak broadness compared to CT NMPF (before ball milling). This diffraction pattern indicates that amorphization is partially progressed in CT-A NMPF thorough coating process, which may leads the degradation of electrochemical performance. To recover crystallinity of CT-A NMPF, reheating treatment was performed at 500°C for 5h under Ar atmosphere. Hereafter, the re-heated CT-A NMPF calls as CT-B NMPF for convenience. XRD pattern of CT-B NMPF is presented in Fig. 6. c. The intensity and broadness of peaks are recovered to same grade as CT NMPF (Fig. 6. a) and no additional peaks are observed. Therefore, the reduced crystallinity by carbon coating is successfully recovered by re-heating treatment without any unexpected side reaction.

The galvanostatic charge-discharge profile of CT-B NMPF is shown in Fig. 7. Discharge capacity is 74 $mAhg^{-1}$ and overpotential during cycling is dramatically improved. The average discharge voltage is 3.8 V that is close to the expected voltage, 4.0 V for NMPF. One can be noticed that only 0.5 Li^+ is electrochemically inserted in NMPF host structure. Even capacity and voltage profile are improved for CT-B NMPF, it is not reached to theoretical value.

As previous study reported, NMPF has no electrochemical activity because of low electric conductivity.[4,5)]

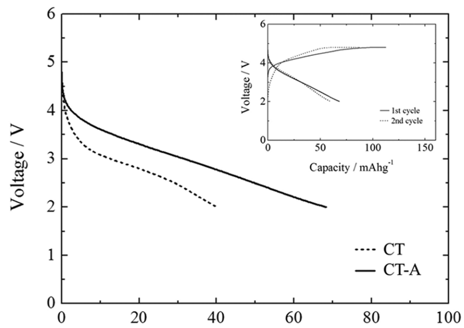

Fig. 5. Discharge profiles for CT-NMPF and CT-A NMPF. Inset shows the charge-discharge profile of CT-A.

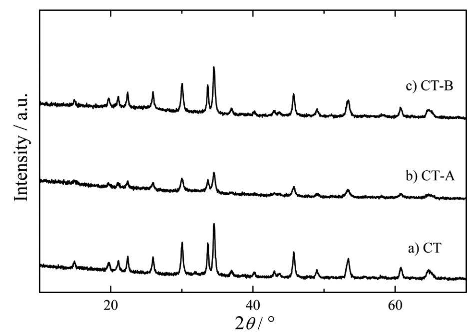

Fig. 6. XRD patterns of NMPFs; a) before carbon coating (CT NMPF), b) after carbon coating (CT-A NMPF), c) after reheat treatment of CT-A (CT-B NMPF).

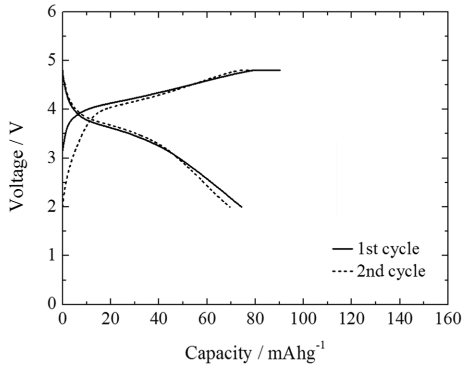

Fig. 7. Charge-discharge profiles for CT-B NMPF (carbon coated then reheated).

Our purpose on this study is to give an electrochemical activity throughout the nano-sized particle and effective carbon coating. Nevertheless, cell performance is not reached to theoretical capacity of 302 mAhg^{-1} even CT-B NMPF sample. In order to confirm the reversible amount of Li^+ participated in insertion/ extraction reaction, high temperature charge-discharge measurement was performed at 60°C within cut off range of 2.0 V to 4.8 V. Fig. 8 presents the discharge profile of CT-B NMPF at 25°C and 60°C. 4.0 V plateau is obviously observed at high temperature discharging and specific discharge capacity is increased to 134 mAhg^{-1}. It is noted that almost 1 Li^+ is electrochemically inserted in NMPF host structure. This result indicates that low specific capacity of NMPF is mainly due to the slow Li^+ diffusion kinetics of NMPF.

As we mentioned, NMPF contains two alkali ions in host structure, so two electron reaction is expected by two Li^+ insertion / extraction reaction. Recently, Kang et.al. reported the reaction voltages of Mn fluorophosphates by first principle calculation.[10] Their results indicate that calculated working voltages over 1 Li^+ or 1 Na^+ insertion ($1 < x < 2$ in $AxMnPO_4F$) are 4.67 V and 4.85 V, respectively. The applied cut-off voltage in this study is 2.0 V to 4.8 V. Therefore, one electron reaction may occur in this voltage range according to the results of first principle simulation. The specific capacity of 134 mAhg^{-1} obtained at high temperature is also close to one Li^+ insertion reaction.

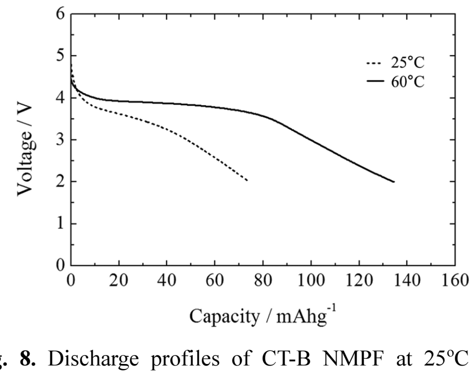

Fig. 8. Discharge profiles of CT-B NMPF at 25°C and 60°C.

We confirm that two Na^+ are extracted from NMPF by chemical oxidation method. However, commercial electrolyte is not stable over high voltage of 4.8 V because of decomposition of electrolyte, which limits to use NMPF as cathode material for 2 electron reaction with doubled capacity.

4. Conclusions

The nano-sized NMPF was successfully synthesized by CT method. The electrochemical inactivity of NMPF due to low electric conductivity was overcome throughout effective carbon coating on nano-sized particles of NMPF. Furthermore, the reduced crystallinity during carbon coating was recovered by re-heat treatment then, the enhanced electrochemical properties were obtained. Only one Li^+ insertion/extraction reaction is possible to progress within the voltage range of 2.0 V to 4.8 V. In order to achieve high capacity due to 2 Li^+ insertion / extraction reaction on NMPF, higher charging voltage over 4.8 V is required. NMPF will be attractive material as high energy cathode, when stable electrolyte at high voltage is launched in the future.

References

1. M. Armand and J-M. Tarascon, *Nature*, **451**, 652 (2008).
2. P.G. Bruce, B. Scrosati, J-M. Tarascon, *Angew. Chem. Int. Ed.*, **47**, 2930 (2008).
3. B.L. Ellis, W.R.M. Makahnouk, Y. Makimura, K. Toghill, and L.F. Nazar, *Nat. Mater.*, **6**, 749 (2007).
4. N. Recham, J-N. Chotard, L. Dupont, K. Djellab, M. Armand, and J-M. Tarascon, *J. Electrochem. Soc.*, **156**, A993 (2009).
5. B.L. Ellis, W.R.M. Makahnouk, W.N.R. Weetaluktuk, D.H. Ryan, and L.F. Nazar, *Chem. Mater.*, **22**, 1059 (2010).
6. T.N. Ramesh, K. Lee, B.L. Ellis, and L.F. Nazar, *J. Electrochem. Soc.*, **13**, A43 (2010).
7. N. Recham, J-N. Chotard, J-C. Jumas, L. Laffont, M. Armand, and J-M. Tarascon, *Chem. Mater.*, **22**, 1142

(2010).
8. D. Wang, J. Xiao, W. Ku, Z. Nie, C. Wang, G. Graff, and J-G. Zhang, *J. Power Sources*, **196**, 2241 (2011).
9. X. Wu, J. Zheng, Z. Gong, and Y. Yang, *J. Mater. Chem.*, **21**, 18630 (2011).
10. S.-W. Kim, D.-H. Seo, H. Kim, K.-Y. Park, and K. Kang, *Phys. Chem. Chem. Phys.*, **14**, 3299 (2012).
11. A.K. Padhi, K.S. Nanjundaswamy, J.B. Goodenough, *J. Electrochem. Soc.*, **144**, 1188 (1997).
12. A. Yamada, S.C. Chung, and K. Hinokuma, *J. Electrochem. Soc.*, **148**, A224 (2001).
13. H. Huang, S.C. Yin, and L.F. Nazar, Electrochem. *Solid State Lett.*, **4**, A170 (2001).
14. T. Shiratsuchi, S. Okada, T. Doi, and J. Yamaki, *Electrochim. Acta*, **54**, 3145 (2009).
15. O.V. Yakubovich, O.V. Karimova, and O.K. Mel'nickov, *Acta Cryst.*, **C53**, 395 (1997).
16. Inorganic Crystal Structure Database, Fach information szentrum (FIZ) Karlsruhe.
17. F. Izumi and K. Momma, *Solid State Phenom.*, **130**, 15 (2007).
18. G. Li, H. Azuma, and M. Tohda, *Electrochem. Solid State Lett.*, **5**, A135 (2002).
19. M. Yonemura, A. Yamada, Y. Takei, N. Sonoyama and R. Kanno, *J. Electrochem. Soc.*, **151**, A1352 (2004).